Advances in
Bridge Engineering

ORIGINAL INNOVATION

Open Access

A softened membrane model for single-box multi-cell composite box-girders with corrugated steel webs under pure torsion

Kongjian Shen[1,2*], Shui Wan[2], Yingbo Zhu[3], Debao Lyu[2] and Zhiqiang Wu[2]

*Correspondence:
aimingskj@gmail.com
[2] School of Transportation, Southeast University, Nanjing 210096, China
Full list of author information is available at the end of the article

Abstract

To analyze the nonlinear torsional behavior of single-box multi-cell prestressed concrete (PC) or reinforced concrete (RC) composite box-girders with corrugated steel webs (BGCSWs), a new theoretical model called unified softened membrane model for torsion (USMMT) is proposed in this study. It is developed from the softened membrane model for torsion which was formerly proposed for the torsional analysis of single-box single-cell PC/RC composite BGCSWs. This proposed model incorporates the different contributions of inner and outer corrugated steel webs (CSWs) in the multi-cell BGCSW to the torsional capacity by introducing a rational relationship of shear strains between inner CSWs and outer CSWs. The satisfactory accuracy of the proposed model is obtained when comparing with the experimental and the finite element analysis results, including the torque-twist curves and the smeared shear strains in concrete slabs and CSWs in the full-range torsional analysis. The comparison indicates that the proposed model is capable of predicting the overall torsional behavior of single-box multi-cell BGCSWs.

Keywords: Single-box multi-cell box-girders, Corrugated steel webs, Softened membrane model, Nonlinear torsional analysis, Torque-twist curve, Shear strain

1 Introduction

The composite box-girders with corrugated steel webs (BGCSWs) have been extensively applied in bridge engineering (Zhu 2020; Corrugated Steel-Web Bridge Association 2021) since the first bridge was built in France in1986 (Cheyrezy and Combault 1990), for which they show many remarkable advantages over the concrete box-girders, such as light weight, high prestress efficiency and few web cracks (Jiang et al. 2015; He et al. 2021). Currently, this kind of steel-concrete composite structures have been used in the design of multi-cell box-girders or curved box-girders (Liu et al. 2021) for satisfying the rapid increasing of traffic demand. But on the other hand, the reduction of torsional stiffness of such structures is about 60–70% of that of the conventional concrete box-girders (Prestressed Concrete Technology Association 2005), leading to a great attention to the research of the torsional behavior of BGCSWs until now (Li 2017).

In recent years, some researchers have introduced the unified theory of concrete structures (Hsu and Mo 2010) into the nonlinear torsional analysis of BGCSWs. These theoretical models can be divided into two types according to their characteristics (Shen et al. 2018a, b): rotating angle torsional theory and fixed angle torsional theory. The typical development path of the application of unified theory of concrete structures into the nonlinear torsional analysis of BGCSWs is shown in Fig. 1.

1.1 Review of rotating angle torsional theory for BGCSWs

In the beginning, the rotating-angle softened truss model for torsion (RA-STMT) in prestressed concrete (PC) structures (Hsu and Mo 1985) was extended to the nonlinear torsional analysis of PC composite BGCSWs (Mo et al. 2000) owing to its features of high solving efficiency and simple mechanics concept. It assumed the shear strains in CSWs to be the same as those in concrete slabs to consider the torsional contribution of CSWs. Then a step-by-step procedure was developed to make a torsional design of PC composite BGCSWs (Mo and Fan 2006). Some researchers (Nie and Tang 2007a) believed that the shear flows in CSWs and concrete slabs should be the same during the twisting of BGCSWs. The RA-STMT was also employed in the torsional analysis of BGCSWs in the post-cracking stage, combining a correction in the pre-cracking stage (Shen et al. 2017).

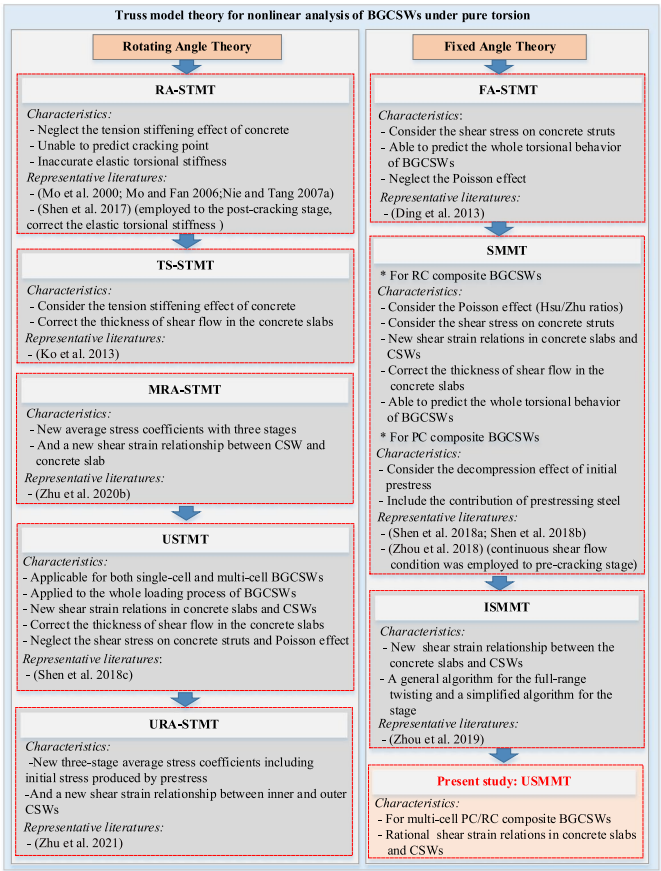

Fig. 1 Progress of the theoretical models for nonlinear torsional analysis of BGCSWs

Note that the RA-STMT is unable to predict the torsional behavior before the cracking of concrete, a tension-stiffened softened truss model for torsion (TS-STMT) was accordingly developed by considering the tension stiffening effect of concrete (Ko et al. 2013). To better predict the torsional behavior at the cracking stage and ultimate stage, the new average stress coefficients with three stages and a new shear strain relationship between CSW and concrete slab were considered in a modified rotating angle softened truss model (MRA-STMT) (Zhu et al. 2020b).

To predict the torsional behavior of single-box multi-cell BGCSWs, a unified softened truss model for torsion (USTMT) (Shen et al. 2018c) was proposed on the basis of RA-STMT by introducing the new shear strain relationships between the CSWs of multi-cell BGCSWs (Shen et al. 2018d). Subsequently, the new three-stage average stress coefficients including initial stress produced by prestress and a new shear strain relationship between inner and outer CSWs were introduced to predict the torsional behavior of multi-cell BGCSWs (Zhu et al. 2021). With the rational modifications, the new model, unified RA-STMT (URA-STMT), can better predict the torsional behavior in the pre-cracking stage.

1.2 Review of fixed angle torsional theory for BGCSWs

While the modified USTMT can well predict the overall mechanical performance of BGCSWs under torsion, such as the torque, twist, and smeared shear strain, it is incapable of explaining the contribution of shear stress on the interface of concrete cracks. Hence, the fixed angle softened truss model for torsion (FA-STMT) in reinforced concrete (RC) structures (Nie and Tang 2007b) was then extended to the torsional analysis of PC composite BGCSWs (Ding et al. 2013). Furthermore, to describe the biaxial strains which consider the Poison effect (Hsu/Zhu ratios), the fixed-angle softened membrane model for torsion (SMMT) (Jeng and Hsu 2009) was introduced to the torsional analysis of single-box single-cell PC/RC composite BGCSWs (Shen et al. 2018a, b). In the same year, different from assuming that the shear strains in the concrete slabs and CSWs before the yielding of CSWs, the continuous shear flow condition was employed to extend the SMMT to the torsional analysis of PC composite BGCSWs (Zhou et al. 2018). Then the algorithms with a new solution process were developed in the improved SMMT (ISMMT) (Zhou et al. 2019), including a general algorithm for the full-range twisting and a simplified algorithm for the stage when the girder was all in the elastic state. These research has shown that the SMMT theory can produce better accuracy in describing the real stress state of concrete in the torsional analysis of BGCSWs than those models based on rotating-angle theory.

1.3 Research motivation and innovations

From above literature review, it can be obviously found that both rotating-angle STMT theory and SMMT theory can well predict the overall mechanical performance of single-box multi-cell BGCSWs under torsion. But the rotating-angle STMT theory can neither reflect the shear stress on the interface of concrete cracks nor describe the biaxial strains in concrete slabs which considers the Poison effect (Hsu/Zhu ratios), whereas, by contrast, the SMMT theory can almost perfectly address the two problems.

The main objective of this study is to extend the SMMT in single-cell BGCSWs to the torsional analysis of multi-cell BGCSWs. A unified method (USMMT) is proposed and an algorithm is compiled to predict the torsional behavior of both single-cell and multi-cell PC/RC composite BGCSWs. A rational relationship of shear strains between inner CSWs and outer CSWs should also be introduced in the proposed model. The symbols used in the present study are defined in the notation list of Appendix 1.

2 Theoretical model for multi-cell BGCSWs under torsion

2.1 Existing equivalent method for single-box multi-cell box-girder

In previous studies (Fu and Yang 1996; Fu and Tang 2001; Allawi et al. 2017), it was generally assumed that the single-box multi-cell box girder under pure torsion could be decomposed into multiple cells with the same twist, so that torsional analysis could be performed separately. This assumption is reasonable in the elastic torsional analysis, but it will underestimate the torsional resistance of the box-girder in the nonlinear torsional analysis. For example, in a single-box triple-cell box-girder as shown in Fig. 2, the applied torque is carried by the three cells together and can be expressed as $T = \sum_{i=1}^{3} 2A_{0i}q_i$. However, when the areas enclosed by the centerline of the shear flow of the three cells are equal ($A_{01}=A_{02}=A_{03}$), the shear flows are also equal ($q_1=q_2=q_3$), thus giving $T = \sum_{i=1}^{3} 2A_{0i}q_i = 2\sum_{i=1}^{3} A_{0i}q = 2A_0q$. This formulas shows that the single-box triple-cell box-girder can be equivalent to a single-box single-cell box-girder with the same outer contour size.

According to the analysis in previous research (Shen et al. 2018d), this simplified calculation method is reasonable for elastic torsional analysis. In the elastic phase, each cell can work together with a coordinated deformation. The shear strains in concrete slabs decrease from the middle of the cross section to both sides, and the shear strains gradually decrease from the outer CSWs to the inner CSWs. At this stage, the

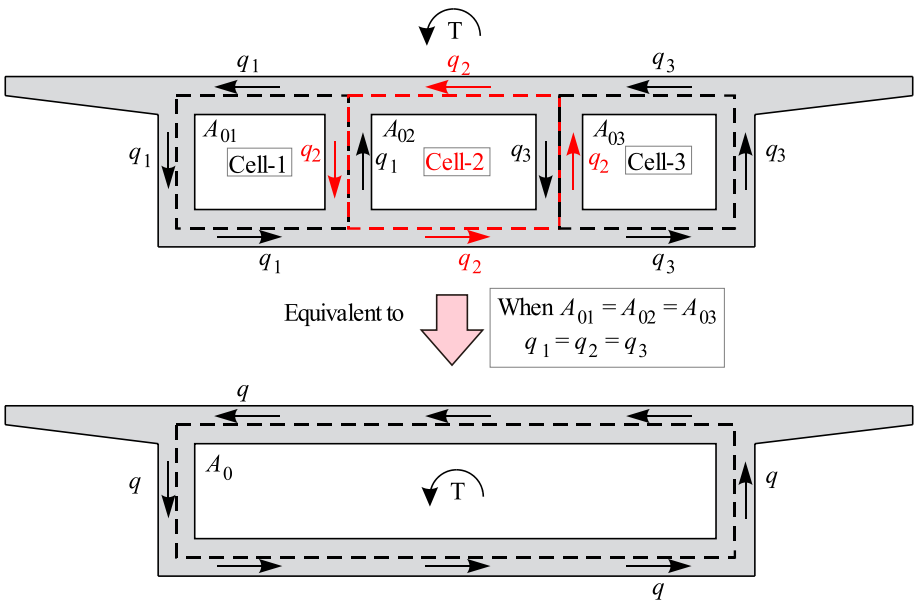

Fig. 2 The shear flows in a single-box triple-cell box-girder

shear strains of the inner corrugated steel webs are small and can be ignored. However, in the non-linear stage after concrete cracking, the shear deformations of the inner webs will also increase greatly in addition to the significant changes in the shear deformation of the outer CSWs. Moreover, the shear deformations of the inner CSWs cannot be ignored in the nonlinear stage, since the outer CSWs will be destroyed first and gradually lose the bearing capacity, and then the inner CSWs will carry a greater load until the failure of the specimens occurs. Therefore, the torsional capacity of the box-girder will be underestimated if only considering the contribution of the outer CSWs to it.

2.2 Rational simplified calculation method for multi-cell BGCSWs under torsion

In the present study, the calculation method for single-box multi-cell BGCSWs under torsion is completely different from the previous simplified method for multi-cell concrete box-girders. The rectangular BGCSW with $2n$ (or $2n$-1) cells was decomposed into n ($n = 1, 2, 3, 4, 5$) pieces of single-box single-cell box girders with the same torsion center as shown in Fig. 3, and then the torsional analysis on each of them were performed. Note that the shear strains in concrete slabs and CSWs in every independent single-cell box can be assumed to be equal before the yielding of CSWs according to the previous research (Mo et al. 2000). Supposing the shear strains (shear stresses) in concrete slab and CSWs of these independent single-cell boxes "Box-i" (i = 1, 2, 3, ..., n) are γ_{lti} (τ_{lti}) and γ_{wi} (τ_{wi}) respectively, the shear strain and shear stress in CSWs of "Box-i" can be obtained as (Shen et al. 2018c):

$$\gamma_{wi} = \begin{cases} R_{\gamma i}\gamma_{lt1}, & \gamma_{wi} < \tau_{wy}/G_e \\ R_{di}\left[(A_{0f1} + A_{0w1})\theta_1 - R_{\gamma i}\gamma_{lt1}b_1\right]/(h_1 - t_{d1}), & \gamma_{wi} \geq \tau_{wy}/G_e \end{cases} \tag{1}$$

$$\tau_{wi} = \begin{cases} G_e\gamma_{wi}, & \gamma_{wi} < \tau_{wy}/G_e \\ \tau_{wy}, & \gamma_{wi} \geq \tau_{wy}/G_e \end{cases} \tag{2}$$

where $R_{\gamma i}$ is the ratio of the shear strain of CSWs in Box-i (γ_{wi}) to the shear train in outermost webs (γ_{w1}). It can be calculated by a fitting formula relating to R_{di} (Shen et al. 2018d), the ratio of the distance between the torsional center and CSWs in Box-i, d_i, to that in the Box-1, d_1:

$$R_{\gamma i} = 0.31215R_{di} + 2.99556R_{di}^2 - 7.29419R_{di}^3 + 4.97228R_{di}^4 \tag{3}$$

It should be noted that Eq. (3) is a fitting formula for simplification, it needs more investigation to better describe the relations among the shear strain of CSWs.

For simplification, the non-uniform shear strain of concrete slab in multi-cell BGCSW is represented by the smeared shear strain of concrete in the Box-1 decomposed from multi-cell BGCSW. It needs to note that this simplification will underestimate the shear strains in concrete slabs, but it can be offset by the overestimation of shear strains in the outermost webs. Then the applied torque of multi-cell BGCSW T_m can be expressed by a unified formula:

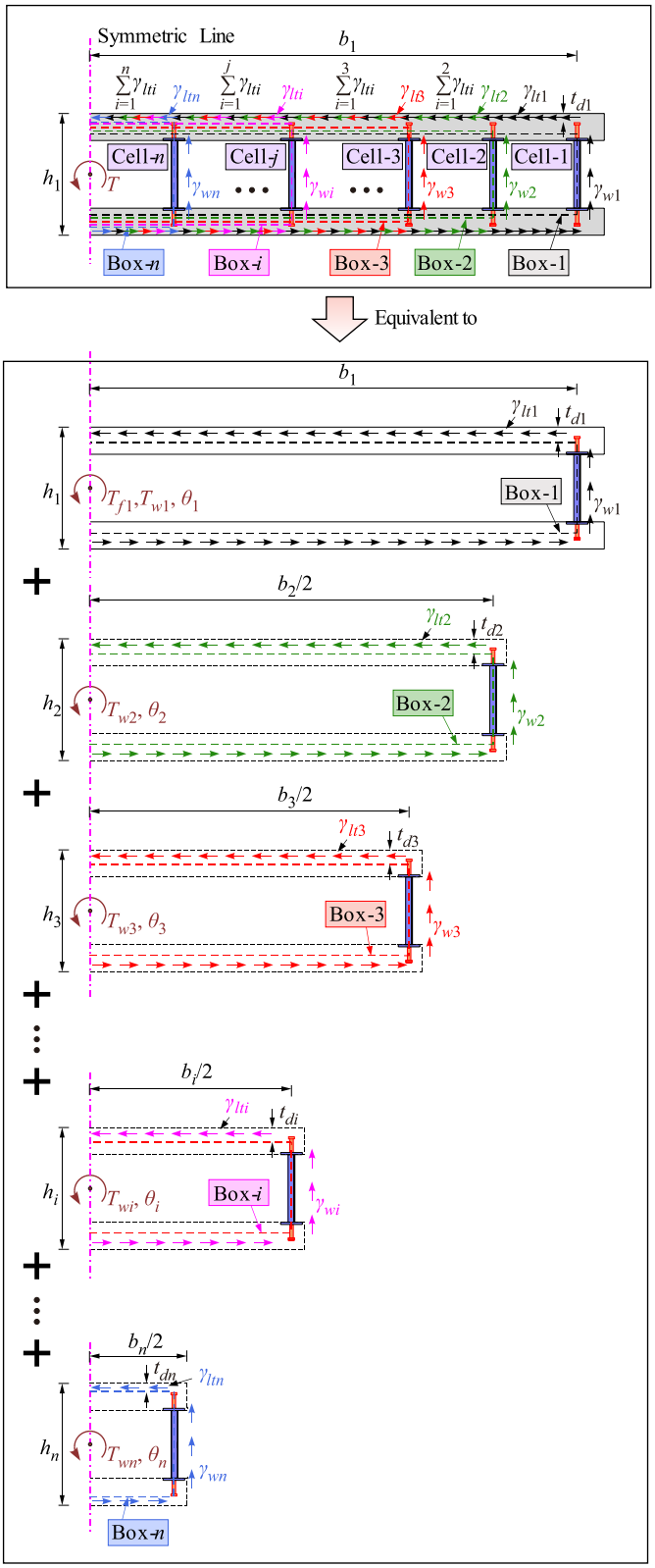

Fig. 3 The equivalence of torsion in the BGCSW with 2*n* (or 2*n*-1) cells

$$T_m = T_{f1} + T_{w1} + \sum_{i=2}^{n} T_{wi},\ m = (2n-1)\ \text{or}\ (2n) \tag{4}$$

where m is a subscript that represents the number of cells in the multi-cell BGCSW; T_{f1} is the torque resisted by the concrete slabs in Box-1; T_{wi} is the torque resisted by the webs in Box-i. They can be calculated by:

$$T_{f1} = 2A_{0f1}\tau_{lt1}t_d \tag{5}$$

$$T_{wi} = 2A_{0wi}\tau_{wi}t_{wi} \tag{6}$$

2.3 USMMT for multi-cell BGCSWs under torsion

The advanced SMMT models for single-box single-cell PC/RC composite BGCSWs under torsion have been proposed by the same authors (Shen et al. 2018a, b). Combining the above calculation formula, the USMMT for torsional analysis of single-box multi-cell PC/RC composite BGCSWs can be obtained, and the solution process is shown as Fig. 4. The relevant equations which have been deduced in the authors' previous researches (Shen et al. 2018a, b) are listed in Appendix 2 to reduce the length of

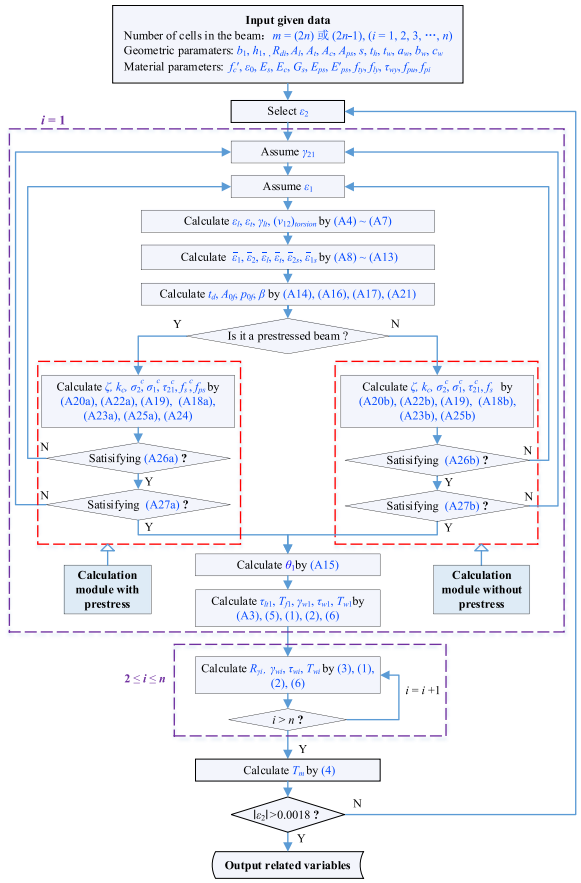

Fig. 4 Flow chart of solution procedure for the USMMT in single-box multi-cell BGCSWs

the main text. From the equations listed in the analysis process of the USMMT for the single-box multi-cell PC composite BGCSWs, it can be seen that there are a total of 32 unknown parameters. (ε_2, ε_1, γ_{21}, ε_l, ε_t, γ_{lt}, $(\nu_{12})_{torsion}$, $\overline{\varepsilon}_1$, $\overline{\varepsilon}_2$, $\overline{\varepsilon}_l$, $\overline{\varepsilon}_t$, $\overline{\varepsilon}_{2s}$, $\overline{\varepsilon}_{1s}$, t_d, A_{0f}, p_{0f}, k_c, β, ζ, σ_2^c, σ_1^c, τ_{21}^c, f_s^c, f_{ps}, θ_1, τ_{lt1}, T_{f1}, $R_{\gamma i}$, γ_{wi}, τ_{wi}, T_{wi}, T_m), 31 effective Eqs. ((1) ~ (6), (9) ~ (40)). In order to solve these unknown parameters, a series of values of ε_2 should be first selected, and then the remaining 31 unknown parameters can be solved with 31 effective equations using the trial and error method. For the non-prestressed single-box multi-cell RC composite BGCSWs, the prestress values just need to be set as zero in this algorithm, which means no prestress is applied. The specific solution process is as follows:

(1) Enter the given parameters, including the cell number of single-box multi-cell BGCSW ($m=2n$) or ($2n$-1), $i=1, 2, 3, \ldots, n$), geometric parameters (b_1, h_1,R_{di}, A_l, A_t, A_c, A_{ps}, s, t_h, t_w, a_w, b_w, c_w), material parameters (f_c', ε_0, E_s, E_c, G_s, E_{ps}, E'_{ps},f_{ty},f_{ly}, τ_{wy},f_{pu},f_{pi}).

(2) Select the initial value of ε_2, which can be varied from 0 to –0.0018 monotonically by an increment of -0.0000001.

(3) Analyze the torsional behavior of the concrete slabs and CSWs in Box-1.

Step 1. Assume γ_{21}.
Step 2. Assume ε_1.
Step 3. Calculate ε_l, ε_t, γ_{lt}, $(\nu_{12})_{torsion}$ according to Eqs. (10) ~ (13).
Step 4. Calculate $\overline{\varepsilon}_1$, $\overline{\varepsilon}_2$, $\overline{\varepsilon}_l$, $\overline{\varepsilon}_t$, $\overline{\varepsilon}_{2s}$, $\overline{\varepsilon}_{1s}$ according to Eqs. (14) ~ (19).
Step 5. Calculate t_d, A_{0f}, p_{0f}, β according to Eqs. (20), (22), (23), (29).
Step 6. Determine whether the BGCSW is prestressed. If yes, proceed directly to the next step; if not, skip to step 10.
Step 7. Calculate ζ, σ_2^c, σ_1^c, τ_{21}^c, f_s^c, f_{ps} according to Eqs. (24), (26), (27), (30), (32), (34), (35).
Step 8. Determine whether the convergence criteria (37) is satisfied. If yes, proceed directly to the next step, if not, return to step 2.
Step 9. Determine whether the convergence criteria (38) is satisfied. If yes, skip to step 13, if not, return to step 1.
Step 10. Calculate ζ, k_c, $k_p\sigma_2^c$, σ_1^c, τ_{21}^c, f_s according to Eqs. (25), (26), (28), (31), (33), (36).
Step 11. Determine whether the convergence criteria (37) is satisfied, if yes, proceed directly to the next calculation, if not, return to step 2;
Step 12. Determine whether the convergence criteria (37) is satisfied, if yes, skip to step 13, if not, return to step 1;
Step 13. Calculate θ_1 according to Eq. (21);
Step 14. Calculate τ_{lt1}, T_{f1}, γ_{w1}, τ_{w1}, T_{w1} according to Eqs. (1), (2), (5), (6), (9).

(4) Analyze the torsional mechanical behavior of the corrugated steel web in the range of $2 \le i \le n$.

Step 15. Let $i=2$;

Step 16. Calculate R_{yi}, γ_{wi}, τ_{wi}, T_{wi} according to Eqs. (1), (2), (5), (6), (9);
Step 17. Determine whether $i > n$ is satisfied. If yes, proceed directly to the next step, if not, set $i = i + 1$, and return to step 16.

(5) Calculate the total torque T_m according to Eq. (4).
(6) Determine whether it meets $|\varepsilon_2| > 0.0018$. If yes, output the required data and stop the calculation. If not, return to section (2) and select the next value of ε_2.

Using above method, the required parameters can be obtained through continuous iterative calculations in an algorithm. Obviously, the USMMT can not only predict the torsional behavior of a single-box multi-cell BGCSW, but also the torsional behavior of a single-box single-cell BGCSW. What's more, it can also both predict the torsional behavior of the PC/RC composite BGCSWs. In the calculation module with prestress, the effect of initial strains and stresses on the constitutive laws of concrete is considered.

3 Model verification with experimental results

3.1 Experimental specimens

In order to validate the proposed unified model, the experimental data of six pieces of single-box multi-cell BGCSWs available from literatures are collected. These specimens were tested under pure torsion, including two single-box double-cell BGCSWs named T-2C (Shen et al. 2018d) and T-2C-S (Shen et al. 2018a), two single-box triple-cell BGCSWs named T-3C (Shen et al. 2018d) and S-3 (Zhu et al. 2020c), two single-box five-cell BGCSWs named S-5 and SU-5 (Zhu et al. 2020c).

Moreover, to better understand the torsional behavior of single-box multi-cell BGCSWs, a specimen named T-3C-S was also tested by the authors after the torsion experiment of specimen T-3C. The test situation of T-3C-S, including the physical parameters and the experimental procedure, is almost the same to that of T-3C except the different yield tensile stress of CSW, thus the relevant information of this specimen will not be repeated in this study.

The geometric and material parameters of all specimens are shown in Table 1. It should be pointed out that the number of tests used to verify the USMMT in this study is relatively small and more torsional test of the specimens with more cells and larger sizes are still needed.

3.2 Torque-twist curves

Figure 5 shows the comparisons of the torque-twist curves of all test beams under pure torsion between the experimental results and the calculated results from the USMMT. In these tests, the twists were measured by several displacement meters (DMs) and inclinometers (IMs) respectively. It can be seen that the torque-twist curves calculated by the USMMT are in good agreement with the test results on the overall trend. Furthermore, the calculated and tested values of the torques and twists at the characteristic points of concrete cracking, CSW yielding and ultimate stage of all test beams are listed in Tables 2 and 3. It can be seen that the predicted values of torques and twists at the characteristic points fit the test results well except for the large difference in the values of twists at some characteristic points. Therefore, the comparison shows that the proposed

Table 1 Geometric and material parameters of the specimens

Specimen	$h \times b$ (mm^2)	t_w (mm)	t_h (mm)	f_c'(MPa)	f_{sy} (MPa) ($d = 8$ mm)	f_{sy} (MPa) ($d = 10$ mm)	f_{sy} (MPa) ($d = 12$ mm)	f_{wy} (MPa)	f_u (MPa)	f_{pi} (MPa)
T-2C	450 × 1200	2	80(70)	22.4	326.8	–	384.2	194.5	–	–
T-2C-S	450 × 1200	2	80(70)	22.4	326.8	–	384.2	194.5	–	–
T-3C	450 × 2000	3	100	32.0	517.4	527.1	–	235	1860	821.4
T-3C-S	450 × 2000	3	100	32.0	517.4	527.1	–	280	1860	821.4
S-3	450 × 2000	2	80	26	350	–	–	260	1860	750
S-5	450 × 2000	2	80	26	350	–	–	260	1860	750
SU-5	450 × 2000	2	80	26	350	–	–	260	1860	750

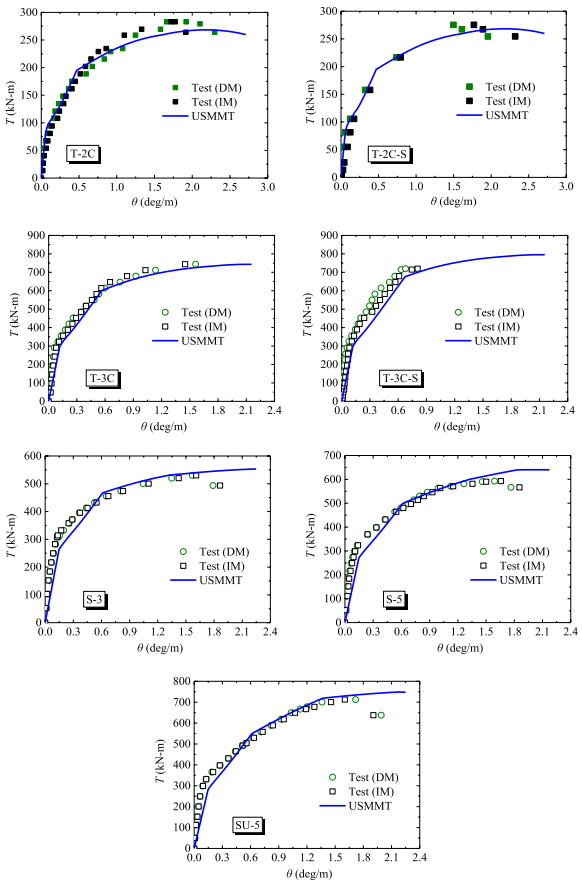

Fig. 5 Comparison of torque-twist curves obtained from tests, and USMMT

Table 2 Prediction accuracy of the USMMT on torques at the characteristic points

Specimen	Cracking state (Concrete)			Yielding state (yielding of CSWs)			Ultimate state (Torque)		
	$T_{cr,exp}$ (kN-m)	$T_{cr,m}$ (kN-m)	$\frac{T_{cr,m}}{T_{cr,exp}}$	$T_{wy,exp}$ (kN-m)	$T_{wy,m}$ (kN-m)	$\frac{T_{wy,m}}{T_{wy,exp}}$	$T_{u,exp}$ (kN-m)	$T_{u,m}$ (kN-m)	$\frac{T_{u,m}}{T_{u,exp}}$
T-2C	94.33	90.22	0.956	175.18	195.12	1.114	282.98	268.33	0.948
T-2C-S	81.39	90.22	1.108	157.93	195.12	1.235	275.43	268.33	0.974
T-3C	242.55	296.75	1.223	614.46	601.76	0.979	743.82	743.28	0.999
T-3C-S	258.72	296.75	1.147	679.14	675.44	0.995	719.57[a]	795.51	1.106
S-3	314.23	263.13	0.837	395.71	466.75	1.180	530.25	553.22	1.043
S-5	323.79	270.13	0.834	431.87	498.05	1.153	592.70	640.31	1.080
SU-5	331.55	281.40	0.849	503.93	548.46	1.088	712.56	748.81	1.051
Mean value			0.993			1.106			1.029
Standard deviation			0.152			0.087			0.053

Note that: *exp* represents the experimental results; *m* represents the predicted values from the USMMT

[a] Due to the limitation of test methods, T-3C-S may not actually reach the ultimate torque

Table 3 Prediction accuracy of the USMMT on twists at the characteristic points

Specimen	Cracking state (Concrete)			Yielding state (yielding of CSWs)			Ultimate state (Torque)		
	$\theta_{cr,exp}$ (°/m)	$\theta_{cr,m}$ (°/m)	$\frac{\theta_{cr,m}}{\theta_{cr,exp}}$	$\theta_{wy,exp}$ (°/m)	$\theta_{wy,m}$ (°/m)	$\frac{\theta_{wy,m}}{\theta_{wy,exp}}$	$\theta_{u,exp}$ (°/m)	$\theta_{u,m}$ (°/m)	$\frac{\theta_{u,m}}{\theta_{u,exp}}$
T-2C	0.129	0.073	0.566	0.428	0.470	1.098	1.769	2.186	1.236
T-2C-S	0.089	0.073	0.820	0.355	0.470	1.324	1.634	2.186	1.338
T-3C	0.058	0.118	2.034	0.578	0.568	0.983	1.506	2.113	1.403
T-3C-S	0.055	0.118	2.145	0.588	0.673	1.145	0.743[a]	2.108	2.837
S-3	0.144	0.148	1.028	0.371	0.612	1.650	1.609	2.249	1.398
S-5	0.134	0.148	1.104	0.430	0.612	1.423	1.657	2.003	1.209
SU-5	0.127	0.148	1.165	0.558	0.612	1.097	1.603	2.182	1.361
Mean value			1.266			1.246			1.540
Standard deviation			0.554			0.215			0.534

[a] Due to the limitation of test methods, this specimen may not actually reach the ultimate torque

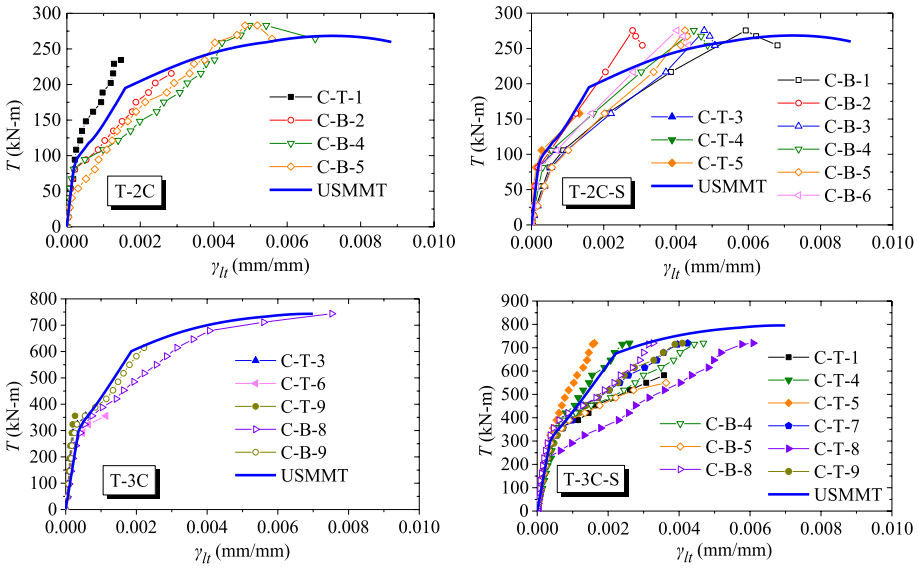

Fig. 6 Comparisons of the shear strains in concrete slabs of the specimens under pure torsion between the experimental results and the calculated results from the USMMT

model in this study can accurately predict the test results of single-box multi-cell PC/RC composite BGCSWs before the ultimate torque is reached.

As shown in Tables 2 and 3, the proposed model has a better prediction on the torques than that on the twists. This is due to the fact that the torques are accurately calculated by Eqs. (5) and (6), however, the twists are roughly calculated by Eq. (21) for analogy to thin-walled circular rod.

3.3 Shear strains in concrete slabs and CSWs

Figures 6 and 7 respectively show the comparisons of the shear strains in concrete slabs and CSWs of the test beam under pure torsion between the experimental results and the calculated results from the USMMT. It should be noted that the shear strains

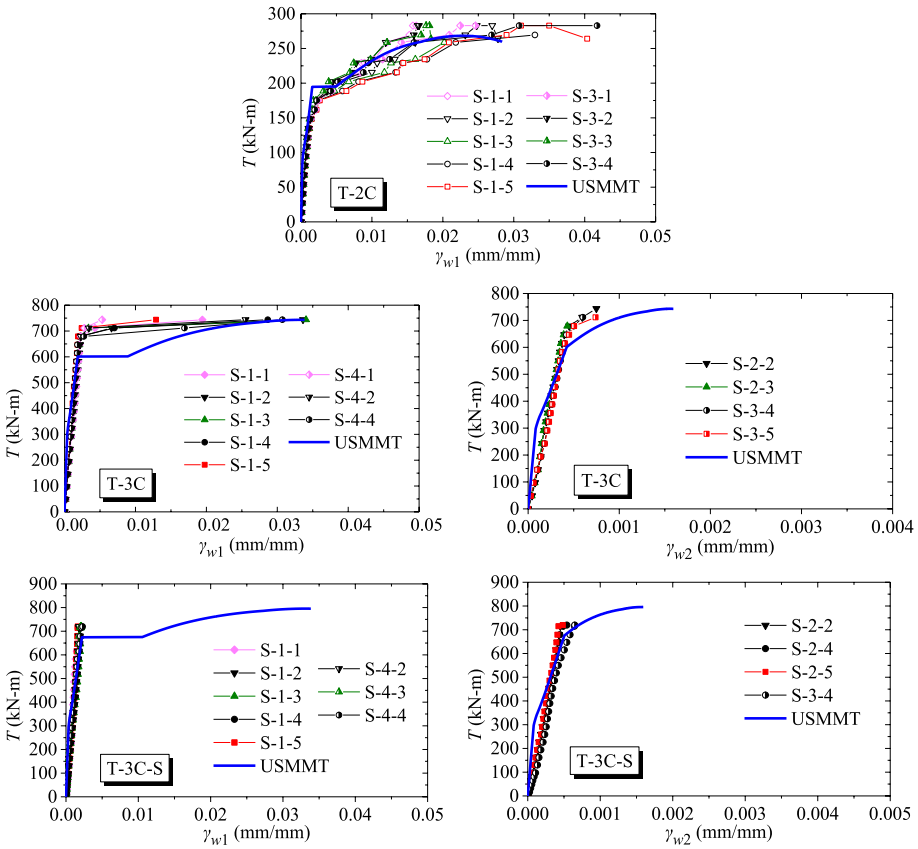

Fig. 7 Comparisons of the shear strains in concrete slabs and CSWs of the specimens under pure torsion between the experimental results and the calculated results from the USMMT

calculated by the USMMT are the average shear strains in concrete slabs and CSWs, whereas the shear strains measured from the test are the shear strains at each measuring point. The shear strains in this study are taken as the absolute values, regardless of the positive and negative values.

In Fig. 6, it can be seen that the calculated results from the USMMT agree well with the test results before the cracking of concrete. Furthermore, the calculated results from the USMMT are basically consistent with the test results after the cracking of concrete in the overall trend, and the predicted values of average shear strains lie between the minimum and maximum tested concrete shear strains at the measuring points.

In Fig. 7, it can be seen that the shear strains of the CSWs are small before the yielding of CSWs, which is similar to the shear strains in concrete slabs. The difference is small between the shear strains measured in the test and the average shear strains in CSWs obtained from Eq. (1). Since the average shear strains in CSWs are assumed to be equal to the average shear strains in concrete slabs in Eq. (1), the curves between the torques and average shear strains in CSWs calculated by the USMMT, however, are broken lines before the yielding of CSWs, which is different from the test results. After the yielding of CSWs, the second assumption in Eq. (1) will cause the average

shear strains in CSWs to have a large abrupt change, which is also different from the test results. Therefore, the assumptions in Eq. (1) still needs to be optimized, but its accuracy needs to be improved though the average shear strains in CSWs obtained from Eq. (1) can roughly reflect the change rules of the average shear strains in CSWs measured in the test. Moreover, the acceptable agreements between the measured shear strains in inner/outer CSWs and the predicted ones demonstrate that the shear strains relationship between the inner CSWs and outer CSWs in Eq. (3) is reasonable.

To sum up, it is reasonable to use the two assumptions in Eq. (1) of the USMMT to express the shear strain relationships between the CSWs and concrete slabs. It can roughly reflect the change rules of average shear strains in concrete slabs and CSWs.

4 Model verification with FEA results

In the previous research (Shen et al. 2018d), a finite element model of the specimen T-3C was established, and its accuracy was verified by test results. Based on the finite element model, the effect of the lateral position distribution of the CSWs and the number of cells on the torsional bearing capacity of the BGCSWs was explored by a parameter analysis. In order to verify the accuracy and applicability of the proposed USMMT, this section will perform a corresponding parameter analysis and compare the calculated results from USMMT with the FEA results.

Table 4 shows the comparisons of ultimate torques of the single-box multi-cell BGCSWs between the calculated results from the USMMT and the FEA results listed in the literature (Shen et al. 2018d). Furthermore, the ultimate torques from the calculated results of the USMMT and the FEA results are shown in Fig. 8 to display the results more vividly. It can be seen from Table 4 and Fig. 8 that the difference between the predicted values of ultimate torques from USMMT and the ones from FEA is within the allowable range of 10% in engineering for the most of BGCSWs. The mean value of the ratios between the predicted values from USMMT and the ones from FEA in all BGCSWs is 1.029 with the standard deviation of 0.076. Therefore, the unified SMMT model in this study can accurately predict the torsional bearing capacity of the BGCSWs with no more than 10 cells.

Further, the comparisons of the torque-twist curves of BGCSWs among the calculated results from the USMMT, the FEA results and the experimental results are shown in Fig. 9. These BGCSWs have an odd number of cells and an arrangement of CSWs at equal intervals in the transverse direction. It can be seen that the results of the torque-twist curves of the single-box multi-cell BGCSWs predicted by the USMMT are in good agreement with the ones from the FEA results and the test results. In addition, the calculated results from the USMMT show that the torque-twist curve of each single-box multi-cell BGCSWs has little difference in the elastic stage before the cracking of concrete, and the difference of torques at the cracking of concrete is also very small. However, the total torques increase significantly when the number of cells in the box-girders increases after the cracking of concrete. This shows that the inner CSWs have little effect on the total torque before the cracking of concrete, whereas they have a significant influence on the total torque after the cracking of concrete. This change rule is basically consistent with the change rule obtained from the FEA. Therefore, the treatment of the inner CSWs by the USMMT model in this study is reasonable. Equation (4)

Table 4 Prediction accuracy of the USMMT on ultimate torques of various multi-cell BGCSWs

BGCSWs		R_{di}	$T_{u,\,FEA}$	$T_{u,\,m}$	$T_{u,\,m}/T_{u,\,FEA}$
(2*n*-1) or (2*n*)-cell	No.				
1-cell ($n=1, i=1$)	S-1C	1	685.61	670.33	0.978
2-cell ($n=1, i=1$)	S-2C	1	689.47	670.33	0.972
3-cell ($n=2, i=1, 2$)	S-3C-1	1, 1/9	698.87	676.44	0.968
	S-3C-2	1, 2/9	719.14	701.24	0.975
	S-3C	1, 1/3	755.62	743.28	0.984
	S-3C-4	1, 4/9	797.20	790.75	0.992
	S-3C-5	1, 5/9	835.59	823.09	0.985
	S-3C-6	1, 2/3	847.74	853.59	1.007
	S-3C-7	1, 7/9	875.82	884.12	1.009
	S-3C-8	1, 8/9	831.26	914.65	1.100
4-cell ($n=2, i=1, 2$)	S-4C	1, 1/2	823.73	807.67	0.981
5-cell ($n=3, i=1, 2, 3$)	S-5C	1, 3/5, 1/5	882.33	859.23	0.974
	S-5C-1	1, 5/9, 1/9	970.09	829.31	0.855
	S-5C-2	1, 2/3, 1/3	916.32	925.27	1.010
	S-5C-3	1, 7/9, 4/9	851.27	1003.57	1.179
	S-5C-4	1, 8/9, 1/2	967.41	1051.87	1.087
6-cell ($n=3, i=1, 2, 3$)	S-6C	1, 2/3, 1/3	918.77	925.27	1.007
7-cell ($n=4, i=1, 2, 3, 4$)	S-7C	1, 5/7, 3/7, 1/7	973.81	992.77	1.019
	S-7C-1	1, 8/9, 5/9, 2/9	1008.36	1097.26	1.088
	S-7C-2	1, 8/9, 2/3, 1/3	1023.58	1168.13	1.141
8-cell ($n=4, i=1, 2, 3, 4$)	S-8C	1, 3/4, 1/2, 1/4	1014.72	1052.65	1.037
9-cell ($n=5, i=1, 2, 3, 4, 5$)	S-9C	1, 7/9, 5/9, 3/9, 1/9	1036.22	1114.24	1.075
	S-9C-1	1, 8/9, 6/9, 4/9, 2/9	1062.17	1248.33	1.175
10-cell ($n=5, i=1, 2, 3, 4, 5$)	S-10C	1, 4/5, 3/5, 2/5, 1/5	1069.91	1182.09	1.105
Mean value					1.029
Standard deviation (24 samples)					0.076

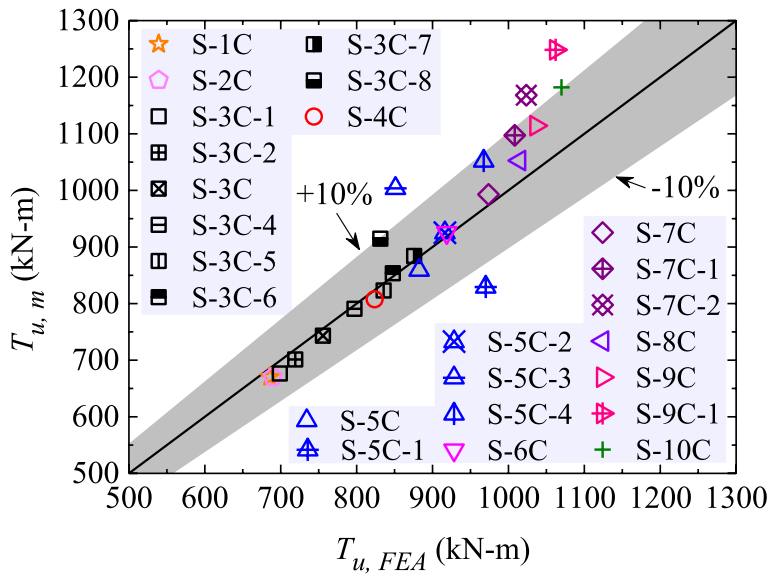

Fig. 8 Comparisons of the ultimate torques between the FEA results and the calculated results from the USMMT

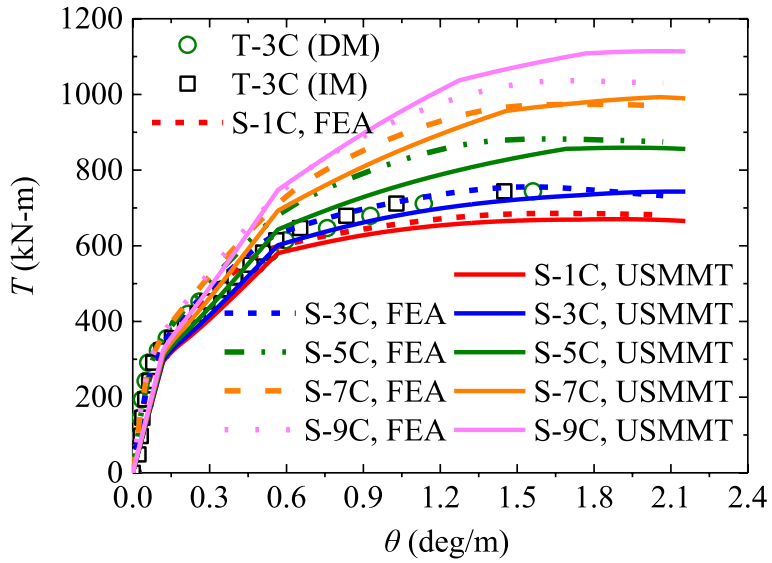

Fig. 9 Comparisons of torque-twist curves between the FEA results and the calculated results from the USMMT

can basically reflect the torsional contribution of the inner CSWs to the total torque of multi-cell BGCSWs.

From above analysis, it can be seen that the proposed model is rational and can be used to predict the overall mechanical properties of the single-box multi-cell PC/RC composite BGCSWs under the action of applied torque, such as the torques, twists, shear strains and so on.

5 Conclusions

In this study, the analytical model SMMT, formerly developed for the single-box single-cell PC/RC composite BGCSWs under pure torsion, is extended to the torsional analysis of single-box multi-cell PC/ RC composite BGCSWs by incorporating the different contributions of the inner and outer CSWs. The proposed model, USMMT for single-box multi-cell PC/RC composite BGCSWs, is verified by the experimental results and the FEA results. The main conclusions can be drawn from the results as follows:

(1) The predicted results from the USMMT agree well with the experimental results and FEA results available in the literature, indicating that the proposed model is able to predict the full-range torsional behavior of single-box multi-cell BGCSWs, such as the torque-twist curves and the torques at the characteristic points.
(2) The proposed model is a unified model that is suitable for both PC and RC composite BGCSWs. It considers the effect of the initial stresses and strains on the constitutive laws of concrete in the calculation module with prestress. As a unified model, it also can predict the torsional behavior of single-cell BGCSWs.
(3) The average shear strains in concrete slabs and CSWs calculated by the USMMT reflect the change rules of shear strains from the test, which validates the reasonability of assumption on the shear strain relations between concrete slabs and CSWs,

as well as the applicability of shear strains relationship formula between inner CSWs and outer CSWs.

It should be admitted that the proposed model is verified by a small number of test specimens and finite element models of the multi-cell BGCSWs with no more than 10 cells, it should be validated by more tests. The shear strain relation between concrete slabs and CSWs and the one between inner CSWs and outer CSWs are still need to be optimized and improved in the future work. This work mainly focuses on a softened membrane model using unified theory, it is suggested by the authors to propose simplified explicit equations in the future to predict the torque and twist for single-box multi-cell composite BGCSWs under pure torsion for practical design.

Appendix 1

T	applied torque of the BGCSW
T_f, T_w	torques contributed by concrete slabs and CSWs, respectively
θ	twist of the BGCSW (angle per unit length), the twist of the box-girder is assumed to be represented by the twist of concrete slabs
b	center distance between CSWs
h	distance between the outer surfaces of upper and lower concrete slabs
t_h, t_w	thickness of concrete slabs and CSWs, respectively
t_d	thickness of shear flow zone in concrete slabs, named effective thickness
d_i	the distance between the torsional center and CSWs in Box-*i*
q,q_i	shear flows in the single-cell and *i*-th cell box-girder, respectively
A_0, A_{0i}	areas enclosed by the centerline of shear flow, q and q_i respectively
A_{0f}, A_{0w}	areas enclosed by the centerline of shear flow in concrete slabs and CSWs, respectively. For rectangular BGCSWs, $A_{0f}=A_{0w}=b(h\text{-}t_d)/2$
p_{0f}	perimeter of the centerline of shear flow, for rectangular BGCSWs, $p_{0f}=2b$
a_w, b_w, c_w	lengths of the flat plate, the projection of inclined plate and the inclined plate, respectively, in one half of wavelength of CSW, l_w
A_c	area of reinforced concrete section, $A_c = 2t_h b$
A_l	total cross-section area of longitudinal (*l*-) steel bars
A_t	cross-section area of one transverse (*t*-) steel bar
A_{ps}	total cross-section area of prestressed tendons
s	spacing of steel bars in the *t*-direction
ρ_s	ratios of steel bars in the *l*- and *t*- directions respectively, ρ_s can be ρ_l or ρ_t, $\rho_l=A_l/(p_{0f}t_d)$, $\rho_t=A_t/(t_d s)$
ρ_{li}, ρ_{pi}	ratios of steel bars and prestressed steel in the *l*- direction with respect to the net area of concrete, respectively, $\rho_{li}=A_l/(A_c-A_l-A_{ps})$, $\rho_{pi}=A_{ps}/(A_c-A_l-A_{ps})$
ρ_{ps}	ratio of prestressed tendons in the *l*- direction, $\rho_{ps}=A_{ps}/(p_{0f}t_d)$
η_w	parameter of corrugation, $\eta_w=(a_w+b_w)/(a_w+c_w)$
μ	Poisson' ratio of steel
β	deviation angle
ζ	softened coefficient of concrete in compression
E_c, E_s, E_{ps}	Young's modulus of concrete, steel bar and prestressing steel, respectively
E_c', E_c''	tensile modulus of concrete before and after the decompression of concrete, respectively
E'_{ps}	initial tangent modulus of Ramberg-Osgood curve
G_s	shear modulus of steel plate, $G_s=E_s(1+\mu)$
G_e	effective shear modulus of CSW, $G_e=G_s\eta_w$
f_c'	cylinder compressive strength of concrete

f_{wy}	yield tensile stress of CSW
f_s	smeared (average) stresses of steel bars induced only by torsion in the *l*- and *t*- directions, respectively, f_s can be f_l or f_t
f_{li}	initial stress of longitudinal steel bars
f_s^c	smeared (average) stresses of steel bars induced by torsion and prestressing in the *l*- and *t*- directions, respectively, f_s^c can be f_l^c or f_t^c
f_{sy}	smeared (average) yield stresses of steel bars in *l*- and *t*- directions, respectively, f_{sy} can be f_{ly} or f_{ty}
f_{ps}	smeared (average) stress of prestressed tendon
f_{pi}	initial stress of longitudinal prestressed tendon
f_{pu}	ultimate strength of prestressing steel
$\sigma_1^c,\ \sigma_2^c$	smeared (average) normal stresses in the 1- and 2-directions, respectively, considering the effect of strain gradient
σ_{ci}	initial compressive stress of concrete caused by prestressing, $\sigma_{ci} = E_c\overline{\varepsilon}_{li}$
τ_{21}^c	smeared (average) shear stress of concrete in 2-1coordinate
τ_{lt}, τ_w	smeared (average) shear stress in concrete slabs and CSWs, respectively
τ_{wy}	yield shear stress of CSW, $\tau_{wy} = f_{wy}/\sqrt{3}$
ε_{cr}, f_{cr}	cracking tensile strain of concrete and its corresponding tensile stress
ε_0	compressive strain at peak concrete strength f_c', taken as -0.002
$\varepsilon_l, \varepsilon_t$	smeared (average) biaxial strains in the *l*- and *t*- directions, respectively
ε_{sy}	smeared (average) biaxial yield strains of steel bars in the *l*- and *t*- directions, respectively, ε_{sy} can be ε_{ly} or ε_{ty}
ε_{sf}	smeared (average) biaxial strain of steel bars which yield first, ε_{sf} can be ε_l or ε_t
$\overline{\varepsilon}_{sn}$	smeared (average) uniaxial yield strain of the steel bars which yield first, $\overline{\varepsilon}_{sn}$ can be $\overline{\varepsilon}_{ln}$ or $\overline{\varepsilon}_{tn}$, $\overline{\varepsilon}_{sn} = (0.93 - 2B_s)\varepsilon_{sy}$
$\overline{\varepsilon}_s$	smeared (average) uniaxial strain induced only by torsion in the *l*- and *t*-directions, respectively, $\overline{\varepsilon}_s$ can be $\overline{\varepsilon}_l$ or $\overline{\varepsilon}_t$
$\overline{\varepsilon}_s^c$	smeared (average) uniaxial strain induced by torsion and prestressing in the *l*- and *t*-direction, respectively, $\overline{\varepsilon}_s^c$ can be $\overline{\varepsilon}_l^c$ or $\overline{\varepsilon}_t^c$
$\varepsilon_2, \varepsilon_1$	smeared (average) biaxial strains in the 2- and 1- directions, respectively
$\overline{\varepsilon}_{1s}, \overline{\varepsilon}_{2s}$	maximum uniaxial strains in the 1- and 2-directions, respectively
$\overline{\varepsilon}_{2s}^c$	maximum uniaxial strains in the 2-direction induced by torsion and prestressing
$\overline{\varepsilon}_1, \overline{\varepsilon}_2$	smeared (average) uniaxial strain in the 1- and 2-directions, respectively
$\overline{\varepsilon}_1^c$	smeared (average) uniaxial strain in the 1-direction induced by torsion and prestressing
$\overline{\varepsilon}_{ps}$	uniaxial strain of prestressing steel
$\overline{\varepsilon}_{pi}$	initial strain of prestressing steel after loss, $\overline{\varepsilon}_{pi} = f_{pi}/E_{ps}$
$\overline{\varepsilon}_{li}$	initial strain of steel bars in the *l*-direction, $\overline{\varepsilon}_{li} = -A_{ps}f_{pi}/\left[A_lE_s + \left(A_c - A_l - A_{ps}\right)E_c\right]$
$\overline{\varepsilon}_{2i},\ \overline{\varepsilon}_{1i}$	initial uniaxial strain in the 2–1 coordinate
$\overline{\varepsilon}_{cx}$	extra strain at the end of decompression of concrete
γ_w	smeared (average) shear strain of CSW
γ_{lt}	smeared (average) shear strain of concrete in the *l*-*t* coordinate
γ_{21}	smeared (average) shear strain of concrete in the 2–1 coordinate
B_s	parameter defined in the constitutive law of mild steel embedded in concrete, B_s can be B_l or B_t, $B_s = (1/\rho_s)\ (f_{cr}/f_{sy})^{1.5}$
$(v_{12})_{torsion}$	Hsu/Zhu ratio used in the SMMT for torsion
k_c	ratio of the average compressive stress to the peak compressive stress
k_t	ratio of the average tensile stress to the peak tensile stress
R_{di}	ratio of the distance between the torsional center and CSWs in Box-*i*, d_i, to that in the Box-1, d_1
R_{yi}	ratio of the shear strain of CSWs in Box-*i*, γ_{wi}, to the shear train in outermost webs, γ_{w1}

Appendix 2

The following equations can be found in the literature (Shen et al. 2018a, b).

(1) In-plane equilibriums in the *l*- and *t*- directions as shown in Fig. 10:

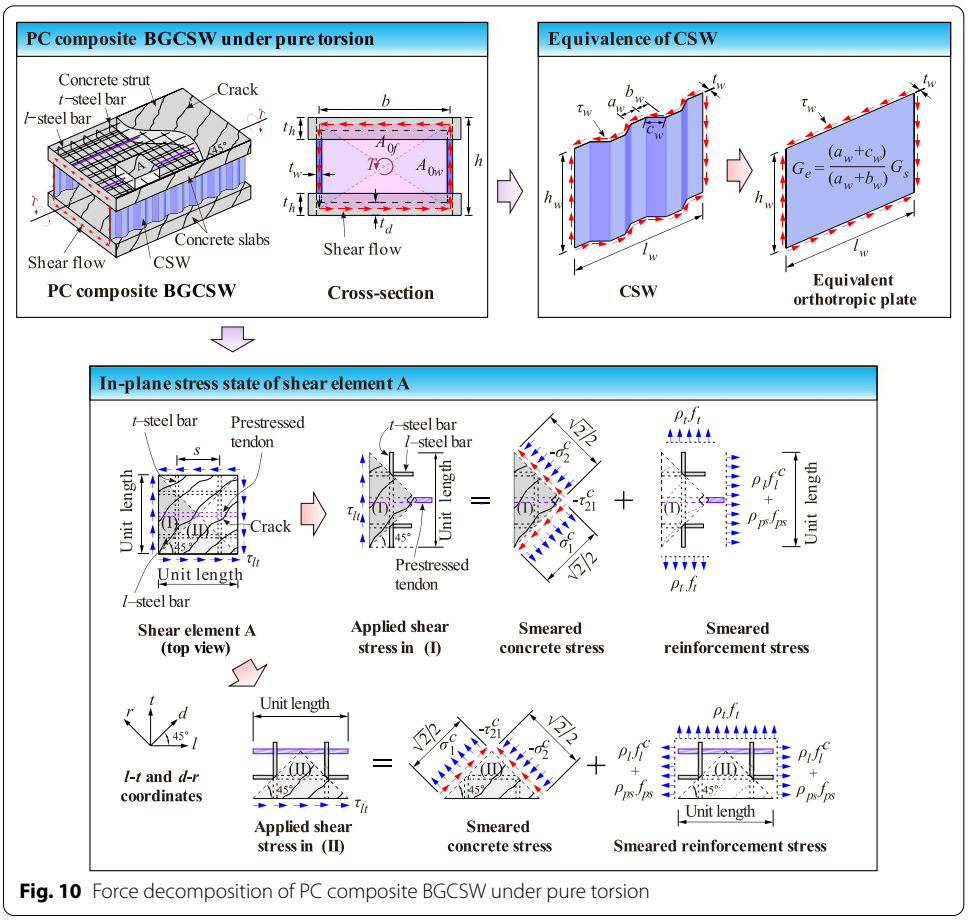

Fig. 10 Force decomposition of PC composite BGCSW under pure torsion

$$\frac{1}{2}\left(\sigma_2^c+\sigma_1^c\right)+\tau_{21}^c+\rho_l f_l=0 \tag{7}$$

$$\frac{1}{2}\left(\sigma_2^c+\sigma_1^c\right)-\tau_{21}^c+\rho_t f_t=0 \tag{8}$$

$$\tau_{lt}=\frac{1}{2}\left(-\sigma_2^c+\sigma_1^c\right) \tag{9}$$

(2) Compatibility equations for concrete slabs:

$$\varepsilon_l=\frac{1}{2}(\varepsilon_2+\varepsilon_1+\gamma_{21}) \tag{10}$$

$$\varepsilon_t = \frac{1}{2}(\varepsilon_2 + \varepsilon_1 - \gamma_{21}) \tag{11}$$

$$\gamma_{lt} = (-\varepsilon_2 + \varepsilon_1) \tag{12}$$

$$(\nu_{12})_{torsion} = \begin{cases} 0.16 + 680\varepsilon_{sf}, & \varepsilon_{sf} \le 0.002 \\ 1.52, & \varepsilon_{sf} > 0.002 \end{cases} \tag{13}$$

$$\overline{\varepsilon}_1 = \varepsilon_1 + \varepsilon_2(\nu_{12})_{torsion} \tag{14}$$

$$\overline{\varepsilon}_2 = \varepsilon_2 \tag{15}$$

$$\overline{\varepsilon}_{2s} = 2\overline{\varepsilon}_2 \tag{16}$$

$$\overline{\varepsilon}_{1s} = 2\overline{\varepsilon}_1 \tag{17}$$

$$\overline{\varepsilon}_l = \frac{1}{2}(\overline{\varepsilon}_2 + \overline{\varepsilon}_1 + \gamma_{21}) \tag{18}$$

$$\overline{\varepsilon}_t = \frac{1}{2}(\overline{\varepsilon}_2 + \overline{\varepsilon}_1 - \gamma_{21}) \tag{19}$$

(3) Effective thickness of the concrete slabs t_d:

$$t_d = \begin{cases} hQ/(Q+4), & t_{d,solid} \le t_h \\ t_h, & t_{d,solid} > t_h \end{cases} \tag{20}$$

where $Q = -2\overline{\varepsilon}_{2s}/\gamma_{lt}$

(4) Relationship between the twist and shear strain in concrete

$$\theta = \frac{p_{0f}}{2A_{0f}}\gamma_{lt} \tag{21}$$

$$A_{0f} = \frac{1}{2}b(h - t_d) \tag{22}$$

$$p_{0f} = 2b \tag{23}$$

(5) Constitutive laws of the concrete in tension:

For prestressed concrete,

$$\sigma_1^c = \begin{cases} \frac{1}{2}\left(E_c'\overline{\varepsilon}_{1s} + \sigma_{ci}\right), & \overline{\varepsilon}_{1s}^c \le \overline{\varepsilon}_{cx} \\ \frac{1}{4}\sigma_{ci}\frac{(\overline{\varepsilon}_{cx} - \overline{\varepsilon}_{1i})}{\overline{\varepsilon}_{1s}} + \frac{1}{2}E_c''\frac{(\overline{\varepsilon}_{1s} + \overline{\varepsilon}_{1i} - \overline{\varepsilon}_{cx})^2}{\overline{\varepsilon}_{1s}}, & \overline{\varepsilon}_{cx} < \overline{\varepsilon}_{1s}^c \le \varepsilon_{cr} \\ \frac{1}{4}\sigma_{ci}\frac{\overline{\varepsilon}_{cx} - \overline{\varepsilon}_{1i}}{\overline{\varepsilon}_{1s}} + \frac{f_{cr}}{2}\frac{\varepsilon_{cr} - \overline{\varepsilon}_{cx}}{\overline{\varepsilon}_{1s}} + \frac{f_{cr}}{0.6}\frac{(\varepsilon_{cr})^{0.4}}{\overline{\varepsilon}_{1s}}\left[(\overline{\varepsilon}_{1s} + \overline{\varepsilon}_{1i})^{0.6} - (\varepsilon_{cr})^{0.6}\right], & \overline{\varepsilon}_{1s}^c > \varepsilon_{cr} \end{cases} \tag{24}$$

where $\overline{\varepsilon}_{cx} = \overline{\varepsilon}_{1i} - \sigma_{ci}/2E_c'$, $E_c' = 2f_c'/\varepsilon_0$, $E_c'' = f_{cr}/(\varepsilon_{cr} - \overline{\varepsilon}_{cx})$.

For reinforced concrete,

$$\sigma_1^c = \begin{cases} \frac{E_c\overline{\varepsilon}_{1s}}{2}, & \overline{\varepsilon}_{1s}/\varepsilon_{cr} \le 1 \\ \frac{E_c\overline{\varepsilon}_{1s}}{2} + \frac{E_c(\varepsilon_{cr})^{1.4}}{0.6\overline{\varepsilon}_{1s}}\left[(\overline{\varepsilon}_{1s})^{0.6} - (\varepsilon_{cr})^{0.6}\right], & \overline{\varepsilon}_{1s}/\varepsilon_{cr} > 1 \end{cases} \tag{25}$$

(6) Constitutive laws of the concrete in compression:

$$\sigma_2^c = -k_c\zeta f_c' \tag{26}$$

For prestressed concrete,

$$\zeta = \begin{cases} 1, & \overline{\varepsilon}_1^c \le 0 \\ \frac{5.8}{\sqrt{f_c'}}\frac{1}{\sqrt{1+400\overline{\varepsilon}_1}}\left(1 - \frac{|\beta|}{24^\circ}\right) \le 0.9, & \overline{\varepsilon}_1^c > 0 \end{cases} \tag{27}$$

For reinforced concrete,

$$\zeta = \frac{5.8}{\sqrt{f_c'}}\frac{1}{\sqrt{1+400\overline{\varepsilon}_1}}\left(1 - \frac{|\beta|}{24^\circ}\right) \le 0.9 \text{ and } \frac{5.8}{\sqrt{f_c'}} \le 0.9 \tag{28}$$

$$\beta(\text{deg}) = \frac{1}{2}\tan^{-1}\left(\frac{\gamma_{21}}{\varepsilon_2 - \varepsilon_1}\right)\frac{180}{\pi} \tag{29}$$

For prestressed concrete,

$$k_c = \begin{cases} \frac{\overline{\varepsilon}_{2s}^c + \overline{\varepsilon}_{2i}}{\zeta\varepsilon_0}\left[1 - \frac{1}{3}\frac{\overline{\varepsilon}_{2s}^c + \overline{\varepsilon}_{2i}}{\zeta\varepsilon_0} + \frac{1}{3}\frac{\overline{\varepsilon}_{2s}^c\overline{\varepsilon}_{2i}}{\zeta\varepsilon_0(\overline{\varepsilon}_{2s}^c + \overline{\varepsilon}_{2i})}\right], & \overline{\varepsilon}_{2s}^c/(\zeta\varepsilon_0) \le 1 \\ \frac{\overline{\varepsilon}_{2s}^c}{\overline{\varepsilon}_{2s}^c - \overline{\varepsilon}_{2i}}\left\{\begin{array}{l}\left[1 - \frac{\zeta^2}{(2-\zeta)^2}\right]\left(1 - \frac{1}{3}\frac{\zeta\varepsilon_0}{\overline{\varepsilon}_{2s}^c}\right) + \frac{\zeta^2}{(2-\zeta)^2}\frac{\overline{\varepsilon}_{2s}^c}{\zeta\varepsilon_0}\left(1 - \frac{1}{3}\frac{\overline{\varepsilon}_{2s}^c}{\zeta\varepsilon_0}\right) \\ -\frac{\overline{\varepsilon}_{2i}^{\,2}}{\zeta\varepsilon_0\overline{\varepsilon}_{2s}^c} + \frac{\overline{\varepsilon}_{2i}^{\,3}}{3(\zeta\varepsilon_0)^2\overline{\varepsilon}_{2s}^c}\end{array}\right\}, & \overline{\varepsilon}_{2s}^c/(\zeta\varepsilon_0) > 1 \end{cases} \tag{30}$$

For reinforced concrete,

$$k_c = \begin{cases} \frac{\overline{\varepsilon}_{2s}}{\zeta\varepsilon_0}\left(1 - \frac{\overline{\varepsilon}_{2s}}{3\zeta\varepsilon_0}\right), & \frac{\overline{\varepsilon}_{2s}}{\zeta\varepsilon_0} \le 1 \\ 1 - \frac{\zeta\varepsilon_0}{3\overline{\varepsilon}_{2s}} - \frac{(\overline{\varepsilon}_{2s} - \zeta\varepsilon_0)^3}{3\overline{\varepsilon}_{2s}(2\varepsilon_0 - \zeta\varepsilon_0)^2}, & \frac{\overline{\varepsilon}_{2s}}{\zeta\varepsilon_0} > 1 \end{cases} \tag{31}$$

(7) Constitutive laws of the concrete in shear:

For prestressed concrete,

$$\tau_{21}^c = \frac{1}{2}\frac{\sigma_1^c - \sigma_2^c}{\varepsilon_1 - \varepsilon_2}\gamma_{21} + \frac{\sigma_{ci}}{2} \tag{32}$$

For reinforced concrete,

$$\tau_{21}^c = \frac{1}{2}\frac{\sigma_1^c - \sigma_2^c}{\varepsilon_1 - \varepsilon_2}\gamma_{21} \tag{33}$$

(8) Constitutive laws of the prestressed steel:

$$f_{ps} = \begin{cases} E_{ps}\overline{\varepsilon}_{ps}, & \overline{\varepsilon}_{ps} \le 0.7f_{pu}/E_{ps} \\ \dfrac{E'_{ps}\overline{\varepsilon}_{ps}}{\left[1+\left(E'_{ps}\overline{\varepsilon}_{ps}/f_{pu}\right)^4\right]^{\frac{1}{4}}}, & \overline{\varepsilon}_{ps} > 0.7f_{pu}/E_{ps} \end{cases} \tag{34}$$

where $\overline{\varepsilon}_{ps} = \left(\overline{\varepsilon}_{pi} - \overline{\varepsilon}_{li}\right) + \overline{\varepsilon}_l^c$.

(9) Constitutive laws of the steel bars embedded in concrete:

For prestressed concrete,

$$f_s^c = \begin{cases} E_s\overline{\varepsilon}_s^c, & \overline{\varepsilon}_s^c \le \overline{\varepsilon}_{sn} \\ (0.91 - 2B_s)f_{sy} + (0.02 + 0.25B_s)E_s\overline{\varepsilon}_s^c, & \overline{\varepsilon}_s^c > \overline{\varepsilon}_{sn} \end{cases} \tag{35}$$

For reinforced concrete,

$$f_s = \begin{cases} E_s\overline{\varepsilon}_s, & \overline{\varepsilon}_s \le \overline{\varepsilon}_{sn} \\ (0.91 - 2B_s)f_{sy} + (0.02 + 0.25B_s)E_s\overline{\varepsilon}_s, & \overline{\varepsilon}_s > \overline{\varepsilon}_{sn} \end{cases} \tag{36}$$

(10) Convergence criteria based on equilibriums:

For prestressed concrete,

$$\rho_l f_l^c + \rho_{ps}f_{ps} - \rho_{li}f_{li} - \rho_{pi}f_{pi} + \rho_l f_t^c = -\left(\sigma_2^c + \sigma_1^c - \sigma_{ci}\right) \tag{37}$$

$$\rho_l f_l^c + \rho_{ps}f_{ps} - \rho_{li}f_{li} - \rho_{pi}f_{pi} - \rho_t f_t^c = -\left(2\tau_{21}^c - \sigma_{ci}\right) \tag{38}$$

For reinforced concrete,

$$\rho_l f_l + \rho_t f_t = -\left(\sigma_2^c + \sigma_1^c\right) \tag{39}$$

$$\rho_l f_l - \rho_t f_t = -2\tau_{21}^c \tag{40}$$

Abbreviations

PC: Prestressed concrete; RC: Reinforced concrete; FE: Finite element; FEA: Finite element analysis; BGCSWs: Box-girders with corrugated steel webs; USMMT: Unified softened membrane model for torsion; CSWs: Corrugated steel webs; RA-STMT: Rotating-angle softened truss model for torsion; TS-STMT: Tension-stiffened softened truss model for torsion; MRA-STMT: Modified rotating angle softened truss model; USTMT: Unified softened truss model for torsion; URA-STMT: Unified rotating-angle softened truss model for torsion; FA-STMT: Fixed angle softened truss model for torsion; SMMT: Softened membrane model for torsion; ISMMT: Improved softened membrane model for torsion; DM: Displacement meters; IM: Inclinometers.

Acknowledgements

The authors would like to thank Pro. Y.L. Mo and Pro. T.T.C. Hsu for their guidance regarding the SMMT theory. All their supports are greatly appreciated.

Authors' contributions

Kongjian Shen: Developing the USMMT theory and corresponding algorithm; performing FEA and parametric study, comparative analysis, writing original draft. Shui Wan: Providing guidance in methodology development, financial supports. Yingbo Zhu: Providing the experimental data and substantially revising the draft. Debao Lyu: Revising and editing the draft. Zhiqiang Wu: Revising and editing the draft. The authors read and approved the final manuscript.

Funding

This study is supported by the National Natural Science Foundation of China (No. 52008095).

Availability of data and materials

The data and materials in current study are available from the corresponding author on reasonable request.

Declarations

Competing interests

The authors declare that they have no competing interests.

Author details

[1]Jiangsu Provincial Transportation Engineering Construction Bureau, Nanjing 210004, China. [2]School of Transportation, Southeast University, Nanjing 210096, China. [3]Department of Civil and Environmental Engineering, University of Pittsburgh, Pittsburgh, PA 15261, USA.

Received: 27 December 2021 Accepted: 24 February 2022
Published online: 12 March 2022

References

Allawi AM, Al-Musawi A, Chai HK, Wan H (2017) Behavior of CFRP strengthened RC multicell box girders under torsion. Struct Eng Mech 61(3):397–406. https://doi.org/10.12989/sem.2017.61.3.397

Cheyrezy M, Combault J (1990) Composite bridges with corrugated steel webs: achievements and prospects. In: Proceedings of the IABSE symposium on mixed structures including new materials, IABSE reports Vol. 60, Brussels

Corrugated Steel-Web Bridge Association (2021) Construction result. http://www.namigata.org/result/.index.html

Ding Y, Jiang KB, Zhou YZ, Yang JK (2013) Analytical model for torsional strength of prestressed concrete box-girder with corrugated steel webs. Chin J Comput Mech 30(1):137–142

Fu CC, Tang Y (2001) Torsional analysis for prestressed concrete multiple cell box. J Eng Mech 127(1):45–51. https://doi.org/10.1061/(ASCE)0733-9399(2001)127:1(45)

Fu CC, Yang DL (1996) Designs of concrete bridges with multiple box cells due to torsion using softened truss model. ACI Struct J 93(6):696–702. https://doi.org/10.14359/516

He J, Wang S, Liu Y, Dai L, Lyu Z, Li C, Xin H, Tan C (2021) The development of composite bridges with corrugated steel webs in China. Proc Inst Civil Eng Bridge Eng 174(1):28–44

Hsu TTC, Mo YL (1985) Softening of concrete in torsional members - prestressed concrete. ACI J Proc 82(5):603–615. https://doi.org/10.14359/10369

Hsu TTC, Mo YL (2010) Unified theory of concrete structures, 2nd edn. Wiley, Chichester

Jeng C, Hsu TTC (2009) A softened membrane model for torsion in reinforced concrete members. Eng Struct 31(9):1944–1954. https://doi.org/10.1016/j.engstruct.2009.02.038

Jiang RJ, Au FTK, Xiao YF (2015) Prestressed concrete girder bridges with corrugated steel webs: review. J Struct Eng 141(040141082). https://doi.org/10.1061/(ASCE)ST.1943-541X.0001040

Ko H, Moon J, Shin Y, Lee H (2013) Non-linear analyses model for composite box-girders with corrugated steel webs under torsion. Steel Compos Struct 14(5):409–429. https://doi.org/10.12989/scs.2013.14.5.409

Li H (2017) Review on torsion and distorsion in prestressed concrete box girders with corrugated steel webs. J Build Struct 38(7):59–67. https://doi.org/10.14006/j.jzjgxb.2017.07.008

Liu S, De Corte W, Ding H, Taerwe L (2021) Mechanical properties of curved composite box girders with corrugated steel webs. Steel Compos Struct 41(1):65–84. https://doi.org/10.12989/scs.2021.41.1.065

Mo YL, Fan Y (2006) Torsional design of hybrid concrete box girders. J Bridg Eng 11(3):329–339. https://doi.org/10.1061/(ASCE)1084-0702(2006)11:3(329)

Mo YL, Jeng C, Chang YS (2000) Torsional behavior of prestressed concrete box-girder bridges with corrugated steel webs. ACI Struct J 97(6):849–859. https://doi.org/10.14359/9630

Nie J, Tang L (2007a) Nonlinear analysis of pure torsion property for prestressed concrete composite box girders with corrugated steel webs. China J Highw Transp 20(5):71–77

Nie J, Tang L (2007b) Nonlinear analysis of reinforced concrete torsional member based on fixed-angle softened truss model. Chin J Comput Mech 24(5):545–549

Prestressed Concrete Technology Association (2005) Design and construction standards of composite bridges. Gihodo Shuppan Co. Ltd, Tokyo

Shen K, Wan S, Jiang Z, Mo Y (2017) Whole process analysis on pure torsional behavior of concrete composite box girders with corrugated steel webs. J Southeast Univ Nat Sci Ed 47(1):112–117

Shen K, Wan S, Mo YL, Jiang Z, Li X (2018c) Behavior of single-box multi-cell box-girders with corrugated steel webs under pure torsion. Part II: theoretical model and analysis. Thin Wall Struct 129:558–572. https://doi.org/10.1016/j.tws.2017.12.023

Shen K, Wan S, Mo YL, Jiang Z, Song A (2018d) Behavior of single-box multi-cell box-girders with corrugated steel webs under pure torsion. Part I: experimental and numerical studies. Thin Wall Struct 129:542–557. https://doi.org/10.1016/j.tws.2017.10.038

Shen K, Wan S, Mo YL, Li X (2018b) A softened membrane model for prestressed concrete composite box girders with corrugated steel webs under pure torsion. Adv Struct Eng 22(2):384–401. https://doi.org/10.1177/1369433218788597

Shen K, Wan S, Mo YL, Li X, Song A (2018a) A softened membrane model for composite box-girders with corrugated steel webs under pure torsion. Eng Struct 173:357–371. https://doi.org/10.1016/j.engstruct.2018.07.021

Zhou C, Li L, Wang L (2019) Improved softened membrane model for prestressed composite box girders with corrugated steel webs under pure torsion. J Constr Steel Res 153:372–384

Zhou C, Li L, Wang L, Shi X (2018) Full-range analysis of prestressed composite box girders with corrugated steel webs subject to pure torsion based on softened membrane theory. China Civil Eng J 51(10):97–106

Zhu Y (2020) Nonlinear behavior of single-box multi-cell composite box-girder with corrugated steel webs under torsion. Master's Dissertation, School of Transportation, Southeast University, Nanjing

Zhu Y, Wan S, Shen K, Su Q, Huang M (2020c) Experimental and numerical study on the nonlinear performance of single-box multi-cell composite box-girder with corrugated steel webs under pure torsion. J Constr Steel Res 168:106005. https://doi.org/10.1016/j.jcsr.2020.106005

Zhu Y, Wan S, Shen K, Su Q, Li X (2020b) Modified rotating-angle softened truss model for composite box-girder with corrugated steel webs under pure torsion. Adv Struct Eng 9(23):1902–1921. https://doi.org/10.1177/1369433219898063

Zhu Y, Wan S, Shen K, Zhou P, Wang X (2021) Theoretical study on the nonlinear performance of single-box multi-cell composite box-girder with corrugated steel webs under pure torsion. J Constr Steel Res 178:106487. https://doi.org/10.1016/j.jcsr.2020.106487

Publisher's Note